

Shortcuts to adiabaticity in superconducting circuits for fast multi-partite state generation

F. A. Cárdenas-López,^{1,2,*} J. C. Retamal,^{3,4} and Xi Chen^{5,6,†}

¹*International Center of Quantum Artificial Intelligence for Science and Technology (QuArtist) and Physics Department, Shanghai University, 200444 Shanghai, China*

²*Forschungszentrum Jülich GmbH, Peter Grünberg Institute, Quantum Control (PGI-8), 52425 Jülich, Germany*

³*Departamento de Física, Universidad de Santiago de Chile (USACH), Avenida Víctor Jara 3493, 9170124, Santiago, Chile*

⁴*Center for the Development of Nanoscience and Nanotechnology, Estación Central, 9170124, Santiago, Chile*

⁵*Department of Physical Chemistry, University of the Basque Country UPV/EHU, Apartado 644, E-48080 Bilbao, Spain*

⁶*EHU Quantum Center, University of the Basque Country UPV/EHU, 48940 Leioa, Spain*

Shortcuts to adiabaticity provides a flexible method to accelerate and improve a quantum control task beyond adiabatic criteria. Here we propose the reverse-engineering approach to design the longitudinal coupling between a set of qubits coupled to several field modes, for achieving a fast generation of multi-partite quantum gates in photonic or qubit-based architecture. We show that the enhancing generation time is at the nanosecond scale that does not scale with the number of system components. In addition, our protocol does not suffer noticeable detrimental effects due to the dissipative dynamics. Finally, the possible implementation is discussed with the state-of-the-art circuit quantum electrodynamics architecture.

I. INTRODUCTION

It has been scrutinized that entanglement [1, 2] in multi-partite quantum systems, plays a crucial role in quantum technologies applications such as quantum information processing [3–5], quantum computation [5, 6], and quantum simulation [7], respectively. Entanglement as a quantum resource can lead to a speed-up in the running time of quantum algorithms [8–11]. Furthermore, the entanglement characterization in many-body systems may provide helpful information concerning whether it is possible to find underlying features of the low-lying energy spectrum with accurate numerical methods [12, 13]. Likewise, entanglement discontinuity is an excellent indicator to characterize phase transitions on quantum systems [14–17]. Besides, in the context of quantum metrology and sensing, using entangled states has achieved quantum-enhanced precision measurements near to the shot-noise limit [18–20], among other applications.

A fundamental condition to generate such multi-partite entangled states relies on the capability of our quantum platform to access a set of interactions or controlled quantum gates that communicate all the system components (all-to-all). Feasibly controllable trapped-ion platform [21] gives a step forward in this direction with the implementation of the so-called Sørensen-Mølmer quantum gate [22–24], where external lasers applied to a confined array of alkali atoms permit access to the red and blue sidebands so that the effective interaction between the ions is of the form $\sigma_{\ell}^x \sigma_{\ell'}^x$ [25, 26].

On the other hand, it is possible to engineer similar interactions in superconducting quantum circuit and circuit quantum electrodynamics (cQED) [27–41], where Josephson junction-based electrical circuits having discrete energy spectrum mimics artificial atoms [42–52], whereas quantized field modes corresponds to either LC resonators, coplanar waveguide or stripline resonator [53–57]. In this architecture, it is possible

to engineer multi-qubit interactions by coupling all of them to a common resonator bus such that in the dispersive regime, we obtain a like-Sørensen-Mølmer interaction [58–61] as a result of a second-order interaction which in principle are slower than the resonant case make them fragile against the unavoidable action with environment [62–65].

Enhanced performance of these protocols may require access to higher coupling strength values where the system operates in the so-called ultrastrong or deep strong coupling regime [66–69]. In such regimes, however, the high hybridization of the energy levels makes it difficult to distinguish between the light and matter degree of freedom. An alternative approach relies on engineering either a pulse sequence or the coupling strength following the ubiquitous methods of shortcut to adiabaticity (STA) [70, 71] that allow us to control a quantum system to accelerate an adiabatic evolution overcoming preparation errors and minimizing the action of the environment [71]. STA has received renewed interest in the context of cQED since it has been generalized to open quantum system [72, 73] permitting to design a counter-diabatic and optimal pulses to speed up a dissipative evolution [74, 75]. Motivated by this, we propose a reverse-engineering method to accelerate the generation of multi-partite entangled states. We design a modulated longitudinal coupling strength that accelerate the generation of multi-partite photonic/qubit states within the nanosecond scale that does not scale with the number of systems (field modes and qubits). Because of the short time, we observe no detrimental effect produced by the action of the environment. Finally, we propose the possible implementation in cQED architecture.

The rest of the paper is organized as follows. In next Sec. II we present our model and Hamiltonian, then in Sec. III describe the fundamental of reverse-engineering method, and propose modulations to generate multi-partite entangled states in a cavity and a set of two-level system. Afterward, in Sec. IV we further discuss the effect of environment on the system dynamics. In Sec. V, the implementation is proposed with superconducting quantum circuits. Finally, our work is concluded in Sec. VI.

* f.cardeans.lopez@fz-juelich.de

† xi.chen@ehu.es

II. MODEL AND HAMILTONIAN

In this section, we will describe the fundamental ingredient in generating multi-partite entangled states. To do so, let us consider a set of N two-level systems of frequency Ω_n coupled to M quantized field modes of frequency ω_m through time-dependent longitudinal coupling $g_n^m(t)$ governed by the following Hamiltonian ($\hbar \equiv 1$)

$$\mathcal{H}_n^m = \sum_n \frac{\Omega_n}{2} \sigma_n^x + \sum_m \omega_m a_m^\dagger a_m + \sum_{n,m} g_n^m(t) \sigma_n^x (a_m^\dagger + a_m), \quad (1)$$

where σ_n^x corresponds to the x -component Pauli matrix characterizing the n -th two-level system, and a_m (a_m^\dagger) stands for the annihilation (creation) bosonic operator of each field mode, respectively. In cQED systems, we can engineer the longitudinal interaction in an artificial atom coupled to a resonator sharing the common external magnetic flux [77, 78], or couple both subsystems through a superconducting quantum interference device (SQUID) [79, 80]. Our implementation is given in Section V.

On the other hand, the structure of the longitudinal coupling between two-level systems with a quantized field mode is suitable for implementing reversed engineering protocols since both interaction and free energy term commutes. Such relation allows us to find an exact adiabatic transformation that accelerates quantum processes such as the qubit readout [75] or implementing faster two-qubit gates [76], and now we will use it to accelerate the generation of multi-partite entangled states of either photonic or qubit states, respectively.

To generate entangled photonic states, we assume that the field modes couple to a single two-level system, i.e., $N = 1$. In such a case, the Hamiltonian reads

$$\mathcal{H}_1^m = \frac{\Omega}{2} \sigma^x + \sum_m \omega_m a_m^\dagger a_m + \sum_m g_1^m(t) \sigma^x (a_m^\dagger + a_m). \quad (2)$$

The Hamiltonian dynamics \mathcal{H}_1^m , in the interaction picture, corresponds to a state-dependent cavity drive represented by the following time-evolution operator

$$U_1^m(t) = \prod_m \hat{\mathcal{D}}_m(\alpha_m(t) \sigma^x), \quad (3)$$

where $\hat{\mathcal{D}}_m(\sigma^x \alpha_m(t)) = \exp(\sigma^x (\alpha_m(t) a_m^\dagger + \alpha_m^*(t) a_m))$ is the displacement operator of the m th field mode with $\alpha_m(t) = -i \int_0^t g_m(s) e^{i\omega_m s} ds$ as the cavity displacement. For a time-independent coupling strength, we obtain that at time $T_k = (2k+1)\pi/\omega_m$ the field mode reaches its maximum displacement $\alpha_{\max} = \pm 2g_1^m/\omega_m$ that depends on the qubit state. Thus, for the system prepared in the initial state $|\Psi(0)\rangle = |g\rangle \otimes_{m=1}^M |0\rangle_m$ ($|g\rangle$ is the ground state of the two-level system, and $|0\rangle_m$ is the vacuum state of the m th field mode) the system evolves to the so-called GHZ cat state [81–84]

$$|\Psi(T)\rangle = \frac{1}{\sqrt{2}} \left[|e\rangle \bigotimes_{m=1}^M |\alpha_{\max}\rangle_m + |g\rangle \bigotimes_{m=1}^M |-\alpha_{\max}\rangle_m \right], \quad (4)$$

by rotating the qubit state along the y axis, we obtain

$$|\Psi\rangle = \frac{1}{\sqrt{2}} \left[|e\rangle \bigotimes_{m=1}^M |\alpha_+\rangle_m + |g\rangle \bigotimes_{m=1}^M |\alpha_-\rangle_m \right], \quad (5)$$

where $|\alpha_\pm\rangle_m = (|\alpha_{\max}\rangle_m \pm |-\alpha_{\max}\rangle_m)/\sqrt{2}$ is the even/odd coherent state superposition [85]. Thus we are lead with a multi-partite hybrid light-matter state embedding maximal entanglement, not being affected by local operations and classical communication (LOCC) [86].

On the other hand, it is possible to generate multi-partite entangled states of qubits when we consider that N two-level systems are coupled to a single field mode described by the Hamiltonian

$$\mathcal{H}_n^1 = \omega a^\dagger a + \sum_n \frac{\Omega_n}{2} \sigma_n^x + \sum_n g_n^1(t) \sigma_n^x (a^\dagger + a). \quad (6)$$

In the interaction picture, the time-evolution operator of \mathcal{H}_n^1 can be written in a factorized form using the Baker-Campbell-Hausdorff (BCH) formula [87]

$$U_n^1(t) = \prod_{n,n'} e^{-iB_{nn'} \sigma_n^x \sigma_{n'}^x} \prod_n e^{-iA_n \sigma_n^x a} \prod_n e^{-iA_n^* \sigma_n^x a^\dagger}. \quad (7)$$

The coefficients $A_n(t)$ ($A_n^*(t)$) and $B_{nn'}(t)$ are obtained calculating the Schrödinger equation for the time-evolution operator $i U_n^1(t) = \mathcal{H}_n^1 U_n^1(t)$. After some calculations, we obtain that these coefficients must satisfy the following differential equations

$$\frac{dA_n(t)}{dt} = g_n^1(t) e^{-i\omega t}, \quad \frac{dB_{nn'}(t)}{dt} = iA_{n'}(t) \frac{dA_n^*(t)}{dt}. \quad (8)$$

For time-independent coupling strength g_n^1 with the initial conditions $A_n(0) = B_{nn'} = 0$, we obtain [59]

$$A_n(t) = \frac{ig_n^1}{\omega} (e^{-i\omega t} - 1), \quad (9a)$$

$$B_{nn'}(t) = \frac{g_n^1 g_{n'}^1}{\omega} [-i(e^{i\omega t} - 1) - t]. \quad (9b)$$

By choosing $\tau = 2\pi/\omega$, the coefficient $A_n(\tau)$ vanishes and $B_{nn'}(\tau) \equiv \theta_{nn'} = 2\pi g_n^1 g_{n'}^1 / \omega^2$. Consequently, the time evolution operator reduces to

$$\begin{aligned} U_n^1(\tau) &= \prod_{n,n'} \exp \left[-i\theta_{nn'} \sigma_n^x \sigma_{n'}^x \right] \\ &= \prod_{n \neq n'} \left[\cos(\theta_{nn'}) \mathbb{I} + i \sin(\theta_{nn'}) \sigma_n^x \sigma_{n'}^x \right], \end{aligned} \quad (10)$$

corresponding to the Sørensen-Mølmer quantum gate [22, 23] (SMG). It is worthy to mention that the SMG has been widely used in the context of quantum simulation to codify fermionic system in a set of coupled two-level system [88, 89]. If we initialize the system in the state $|\Phi(0)\rangle = \bigotimes_{n=1}^N |g\rangle_n \otimes |0\rangle$, and choose $\theta_{nn'} = \pi/4$, the state evolves to a GHZ state [90]

$$|\Phi(\tau)\rangle = \frac{1}{\sqrt{2}} \left[\bigotimes_{n=1}^N |g\rangle_n + e^{i\pi(N+1)/2} \bigotimes_{n=1}^N |e\rangle_n \right] |0\rangle, \quad (11)$$

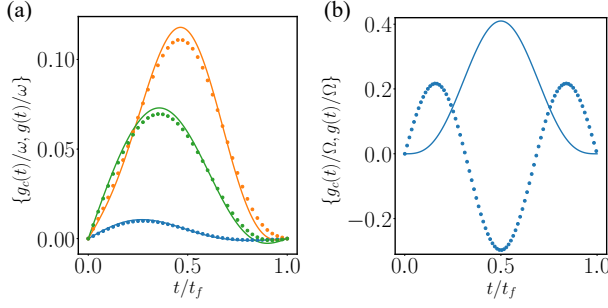


FIG. 1. Reversely engineered coupling strength $g_c(t)$ (continuous line) and $g(t)$ (dotted) as a function of the dimensionless time t/t_f for (a) the GHZ for photonic systems, blue, orange and blue data corresponds to the pulse considering $\alpha(t_f) = 1, 3, 5$, respectively. Whereas (b) stands for the GHZ in qubits. The numerical simulations are preformed with the following system parameters (a) $\omega/2\pi = 6.6$ GHz, $g/2\pi = 21$ MHz, and (b) $\Omega/2\pi = 10$ GHz, $\omega/2\pi = 1$ GHz, and $g/2\pi = 144$ MHz.

Notice that in those derivations, the time generation is constrained by the ratios g_1^m/ω_m , and g_n^1/ω_m , respectively. In particular, it is possible to implement the multi-partite gate for photons in the timescale $T = 47.61$ (ns), whereas for the multi-partite operation with qubits, the gate time is $T = 19$ (ns) [59]. Thus, to obtain faster time generation, we must achieve larger coupling strength values, meaning that the system will operate in the ultra-strong or deep-strong coupling regime [66–69]. A way to accelerate the generation time without demanding larger coupling strength relies upon the technique of STA [71], where the modulation of system parameters or the addition of an additional term on the system dynamics leads to a speedup of the quantum processes. In what follows that we will explore the former alternative, the reverse-engineering method [70, 75], to design the coupling strength g_1^n and g_n^1 such that the gating time is shortened significantly.

III. REVERSE ENGINEERING PROTOCOL

In this section, we will discuss how to design the coupling strengths g_1^n and g_n^1 following the reverse-engineering approach [70, 75]. We will develop the theory considering a single two-level system ($N = 1$) coupled to a single field mode ($M = 1$) with coupling strength $g(t)$, the for many qubits and field modes is easily derivable. In this case, we propose the solution of the Schrödinger equation of the form $|\Psi(x, t)\rangle = \exp(-i\epsilon\mathcal{U}(t))$, where $\epsilon = \omega(n + 1/2)$ and $|\varphi(x, t)\rangle$ correspond to the eigenfunction for the uncoupled cavity with Hamiltonian $\omega_r a^\dagger a$ and $|\xi\rangle$ describes the qubit state. Additionally, $\mathcal{U}(t)$ stands for a unitary transformation that eliminates the qubit-field mode coupling [91–93]

$$\mathcal{U}(t) = e^{i\beta(t)} e^{-ig_c(t)\sigma^x(a^\dagger + a)/\omega^2} e^{-g_c(t)\sigma^x(a^\dagger - a)/\omega}. \quad (12)$$

Here, the overdot notation represents time-derivative, and $\beta(t) = -\int_0^t \mathcal{L}_g(s)ds$ corresponds to a phase factor that re-

lates the coupling strength $g(t)$ with the auxiliary variable $g_c(t)$ through the classical Lagrangian

$$\mathcal{L}_g(t) = \frac{\dot{g}_c^2(t)}{\omega^3} - \frac{g_c^2(t)}{\omega} - \frac{2g_c(t)g(t)}{\omega}. \quad (13)$$

To guarantee that $|\varphi(x, t)\rangle$ corresponds to the exact solution of the time-dependent Schrödinger equation, the classical variable must obey the following equation of motion

$$\ddot{g}_c(t) + \omega^2[g_c(t) + g(t)] = 0, \quad (14)$$

which is nothing but the Euler-Lagrange equation from the classical Lagrangian. The auxiliary variable $g_c(t)$ needs to satisfy the following boundary conditions to guarantee that at the initial/final time, the auxiliary variable does not participate in the system

$$g_c(t_0) = \dot{g}_c(t_0) = \ddot{g}_c(t_0) = 0, \quad (15a)$$

$$g_c(t_f) = \dot{g}_c(t_f) = \ddot{g}_c(t_f) = 0, \quad (15b)$$

Furthermore, we can add more conditions depending on the problem to be solved. For the photonic GHZ, we require that the final cavity displacement be larger as we can at the final time t_f the final cavity displacement be larger than we can. In this scenario, together with the boundary conditions in Eq. (15a) and Eq. (15b), we add the following constrains

$$\alpha(t_f) = -i \int_0^{t_f} g(s) e^{i\omega s} ds = d_{\max}, \quad (16)$$

corresponding to an arbitrary cavity displacement. On the other hand, for the generation of the GHZ state for qubits, apart from the boundary conditions given in Eq. (15a) and Eq. (15b) we require that

$$A_n(t_f) = 0, \quad B_{nn'}(t_f) = \frac{\pi}{4}. \quad (17)$$

We propose a Fourier decomposition as ansätze for the auxiliary variable i.e., $g_c(t) = \sum_k c_k \sin(\pi k t/t_f)$. Notice that this modulation satisfies by itself the conditions $g_c(0) = g_c(t_f) = \dot{g}_c(0) = \dot{g}_c(t_f) = 0$. Therefore, we only require to find the coefficient that fulfill the conditions $\dot{g}_c(t_0) = \dot{g}_c(t_f) = 0$ together with the Eq. (16) for the photonic case, and Eqs. (17) for the qubits, respectively.

We numerically calculate the coefficients c_k using the gradient descent minimization package of python [94]. Fig. 1 shows the auxiliary variable $g_c(t)$ and the coupling strength $g(t)$ obtained through Eq. (14) as a function of the dimensionless time t/t_f for three different maximal cavity displacement $d_{\max} = \{1, 3, 5\}$, respectively. It manifests that the maximal value of the coupling strength $g(t)$ strongly depends on the maximal value of the cavity displacement constraining the coherent state's size, unlike the qubit case, where we do not observe such behavior in the resulting $g_c(t)$ and $g(t)$, respectively. Moreover, it is shown that the modulations obtained in Fig. 1 satisfy the additional conditions stated in Eq. (16) and Eqs. (17) for the photonic and qubit case, respectively. We plot these quantities as a function of the dimensionless time t/t_f depicted in Fig. 2. For the coupling strength $g/2\pi = 21$ MHz [77] for the photonic system, we

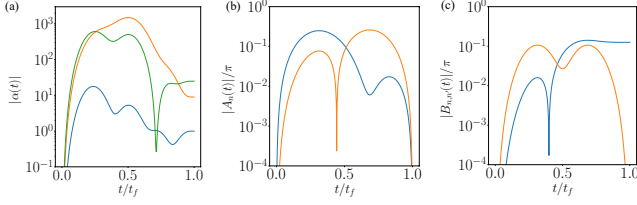


FIG. 2. Reversely engineered (a) absolute cavity displacement $|\alpha(t)|$ as a function of the dimensionless time t/t_f , blue, orange and green lines correspond to the maximal cavity displacement of $d_{\max} = \{1, 3, 5\}$, respectively. (b) and (c) stand for the real (blue) and imaginary (orange) parts of the reversely engineered $|A_n(t)|$ and $|B_{nn'}(t)|$ coefficients, respectively. The numerical simulations are preformed with the same parameters as those in Fig. 1.

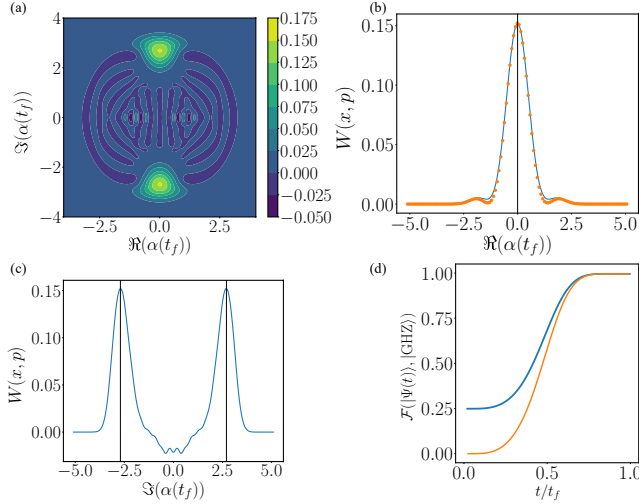


FIG. 3. (a) Wigner representation of the reduced density matrix of the first field mode at final time t_f for a system consisting into three field mode coupled to a single qubit. Projection of the Wigner function to the (b) coordinate space and (c) the momentum space, corresponding to a Gaussian function centered in $\pm d_{\max} = 3$. (d) Fidelity \mathcal{F} between the target GHZ state in Eq. (5) with the state $|\Psi(t)\rangle$ for two different maximal cavity displacement $d_{\max} = 1$ to the blue line, and $d_{\max} = 3$ for the orange line, respectively. The numerical simulations are carried out with the same parameters as those in Fig. 1.

obtain a generation time $t_f = \pi/(40g) \equiv 3.74$ (ns) achieving $\alpha(t_f) = d_{\max}$. Whereas, the qubit-based GHZ state can be generated within the timescale $t_f = \pi\omega/(80g^2) \equiv 1.89$ (ns) for a coupling strength $g/2\pi = 114$ MHz [59] where the conditions $A_n(t_f) = 0$ and $B_{n,n'}(t_f) = \pi/4$ are fulfilled, respectively.

A. Multi-partite photonic state

We analyze the performance of the reversely engineered coupling strength $g(t)$ to generate photonic GHZ states for $M = 3$ modes, see Hamiltonian of Eq. (2). In such a case, we assume that $g_1^m(t) \equiv g(t) \forall m$. We quantify the Wigner func-

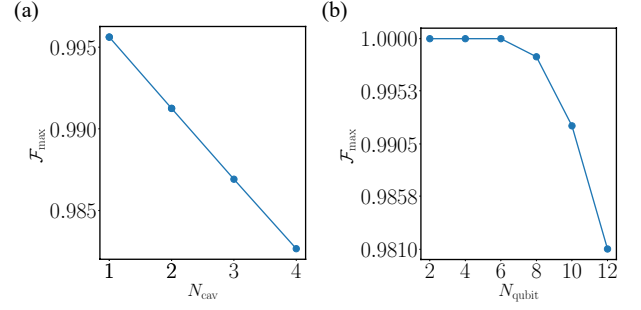


FIG. 4. Fidelity \mathcal{F} at the STA time t_f as a function of the number of system constituents for a system corresponding to (a) one qubit coupled to $M = \{1, 2, 3, 4\}$ field modes with maximal cavity displacement $d_{\max} = 3$, and (b) one field mode coupled to $N = \{2, 4, 6, 8, 10, 12\}$, respectively. The numerical simulations are carried out with the same parameters as those in Fig. 1.

tion $W(x, p)$ of the reduced density matrix of the first field modes given by $\rho_{f_1}(t) = \text{Tr}_{\{f_2, \dots, f_M, q\}}[|\Psi(t)\rangle\langle\Psi(t)|]$, where the sub-indexes f_k , and q corresponds to the partial trace over the k -th field mode and the qubit, respectively. Given that $W(x, p)$ for a coherent state $|\alpha\rangle$ corresponds to a Gaussian centered in $(\text{Re}(\alpha), \text{Im}(\alpha))$ [85], at the final STA time t_f , where $\rho_{f_1}(t_f) = (1/2)(|d_{\max}\rangle\langle d_{\max}| + |-d_{\max}\rangle\langle -d_{\max}|)$, the Wigner function represents two Gaussians centered at $\pm d_{\max}$. Fig. 3(a) shows the Wigner function on the phase space corresponding to two points far apart to each other from a distance $2d_{\max}$. Likewise, Fig. 3(b)-(c) shows the one-dimensional projection of $W(x, p)$ in the coordinate and momentum space, respectively. In concordance with Fig. 3, we appreciate that on the coordinate projection, we should expect to see a single Gaussian centered at zero (no imaginary component on the coherent state) placed at $p = \pm d_{\max}$. In contrast, in the momentum projection, we have to see two overlapping Gaussian centered at $x = \pm d_{\max}$, respectively. From Fig. 3(c) we see a wide region where $W(x, p)$ takes negative values, showing the non-local nature of the multi-partite entangled state [85].

Furthermore, we also calculate the Fidelity $\mathcal{F}(\rho, \sigma) = \text{Tr}[\sqrt{\sqrt{\rho}\sigma\sqrt{\rho}}]^2$ (ρ and σ are arbitrary density matrices) between the state $|\Psi(t)\rangle$ obtained by numerically solve the Schödinger equation of Eq. (2) with the target GHZ state defined in Eq. (5) for $M = 3$ field modes for two different maximal field displacement $d_{\max} = \{1, 3\}$ as depicted in Fig. 3(d). We observe that the reversed engineering protocol is insensitive to the final displacement d_{\max} , where we appreciate fidelities close to one for both modulations.

Thus far, we have demonstrated that our reverse-engineering protocol provides a flexible way to engineer the longitudinal coupling strength that allows us to generate a multi-partite photonic states at a short timescale ($t_f \equiv 3.2$ (ns)), which is one order of magnitude shorter than the same protocol without the use of the reverse engineering approach ($T = 47.61$ (ns)). Moreover, our reverse engineering approach permit us fixing the final cavity displacement beyond the maximal displacement $\alpha_{\max} = \pm 2g_1^m/\omega_m$. Nev-

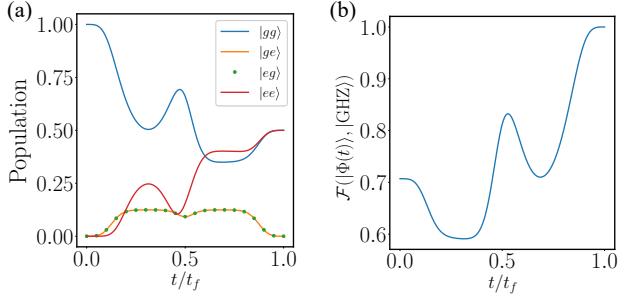


FIG. 5. (a) Population evolution of the two-qubit states $|gg\rangle$ (continuous blue), $|ge\rangle$ (continuous orange), $|eg\rangle$ (dotted green), and $|ee\rangle$ (continuous red) computed from the Hamiltonian in Eq. (6) through the reverse-engineering protocol as a function of the dimensionless time t/t_f , we observe that at final time the state evolves to a GHZ state. (b) Fidelity \mathcal{F} as a function of t/t_f between the GHZ state of two qubits with the state $|\Phi(t)\rangle$. The numerical simulations are carried out with the same parameters as those in Fig. 1.

ertheless, nothing is said about the scaling of the protocol in terms of the number of field modes. We should expect that the gating time t_f does not scale from our calculations. To assure that, we solve the dynamics by increasing the number of field modes from $M = 1$ to $M = 4$ and compute the fidelity $\mathcal{F}(t_f)$ at t_f for each case. Those results are depicted in Fig. 4(a), where we observe a high-fidelity generation of the cat Schödinger states (the maximal fidelities obtained with the protocol are around 98% – 99% for each case). Furthermore, we also see minor variations in the achieved maximal fidelity for the maximal number of modes simulated here. The exploration regarding a higher amount of field modes may be helpful to probe our conjecture. However, we are contained by the maximal displacement that bound the size of the whole Hilbert space, i.e., the maximal size of each field mode is chosen such $N_{\max} = |d_{\max}| + 1$. In this sense, there exists a trade-off between the macroscopic size of the coherent state (related to the maximal displacement) with the maximal number of field modes to be simulated.

B. Multi-partite qubit state

Alternatively, we will analyze the performance of the reverse-engineering protocol to generate GHZ states in a qubit-based system. For doing so, we study the dynamics of the Hamiltonian in Eq. (6) by considering $N = 2$ qubits assuming homogeneous coupling strength between the qubits with the field mode, i.e., $g_n^1(t) = g(t) \forall n$. Then, we can extend the result to a multi-qubit system up to 12 of them.

Similar to the previous section, we look at a reduced part of the Hilbert space corresponding to the reduced density matrix of the N qubits defined as $\rho_q(t) = \text{Tr}_f[|\Phi(t)\rangle\langle\Phi(t)|]$, where the sub-index f corresponds to the trace over the field mode, where $|\Phi(t)\rangle$ is the solution of the Schödinger equation for the Hamiltonian given in Eq. (6). Fig. 5 (a) shows the population evolution for a system composing by $N = 2$ qubits. We see that the occupation probabilities of the symmetric subspace

$\{|ge\rangle, |eg\rangle\}$ does not be equal to zero during all the dynamics because the terms related to their evolution in the time evolution operator given in Eq. (7) is not zero at all the times. In fact, the quantity $A_n(t)$ only vanishes at $t = 0$, and $t = t_f$, respectively. Likewise, the population of the state $|ee\rangle$ keeps changing until t_f achieves its optimal value. In Fig. 5(b) we plot the fidelity \mathcal{F} as a function of time with the target state given in Eq. (11). Since the symmetric state contributes to the whole state's probability, fidelity tends to decrease until it reaches its maximal value around $\mathcal{F} = 99\%$. Concerning the scaling of the generation time for the GHZ state, we obtain that the gating time does not scale with the number of qubits. In order to prove that, we calculate the fidelity \mathcal{F} evaluated at $t = t_f$ by increasing the number of qubits from $N = \{2-12\}$. Fig. 4(b) shows the maximal fidelity as a function of the number of qubits. It is observed that the fidelities \mathcal{F} are bounded between 98% – 99%, thus demonstrating that the gating time does not scale with the number of qubits for achieving a large fidelity.

Notice that in the derivation of the unitary transformation provided in Eq. (10), no approximation has been made, which makes this protocol faster than other proposals based on dispersive interaction corresponding to second-order processes [58, 60, 61]. In this sense, the reverse-engineering protocol of generating these multi-parties entangled states allows us to accelerate its generation leading to generation times shorter than the tenth nanosecond scale, which mitigates the error produced by the unavoidable interaction with the environment. In the next section, we will quantify how the dissipation affects the performance of our protocols.

IV. DISSIPATIVE DYNAMICS

We study the generation of multi-partite entangled states under the losses mechanism, which may be dissipative (energy relaxation) or not as dephasing on the qubits. The system dynamics is described by the Lindblad master equation,

$$\begin{aligned} \frac{d\rho(t)}{dt} = & -i[\mathcal{H}_n^m, \rho(t)] + \sum_{m=1}^M \kappa_m \mathcal{L}[a_m, \rho(t)] \\ & + \sum_{N=1}^N (\gamma_n \mathcal{L}[\sigma_n^-, \rho(t)] + \gamma_{\phi,n} \mathcal{L}[\sigma_n^z, \rho(t)]), \quad (18) \end{aligned}$$

where \mathcal{H}_n^m is the Hamiltonian given in Eq. (1), $\mathcal{L}[\mathcal{O}, \rho(t)] = \mathcal{O}\rho(t)\mathcal{O}^\dagger - \{\mathcal{O}^\dagger\mathcal{O}, \rho(t)\}/2$ is the Lindbladian operator describing the dynamics of a open quantum system [95]. κ_m and γ_n stand for the relaxation ratio of the m -th cavity and the n -th qubits, respectively. Finally, $\gamma_{\phi,n}$ is the dephasing ratio of the n -th qubit. Here, we will focus on the previous cases, where we consider a single-qubit interacting with M modes described by \mathcal{H}_1^m as in Eq. (2), and N qubits interacting with a single cavity characterized by \mathcal{H}_n^1 in Eq. (6). Without loss of generality, we assume homogeneous decay rates for the energy relaxation of the field mode, qubit relaxation, and dephasing rate, i.e., $\kappa_m = \kappa$, $\gamma_n = \gamma$, and $\gamma_{\phi,n} = \gamma_\phi$, respectively. We start by preparing the systems in the following

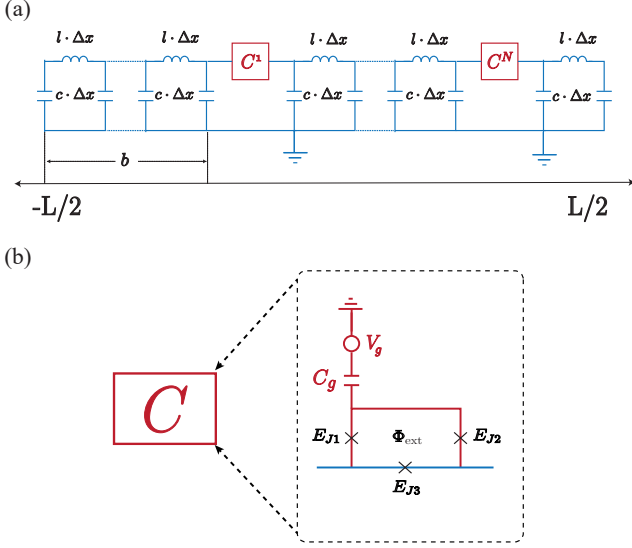


FIG. 6. The schematic illustration of our experimental proposal consists of (a) a $\lambda/2$ coplanar waveguide resonator (CPWR) galvanically coupled to (b) N artificial atoms, namely C^n formed by a superconducting loop interrupted by three Josephson junctions threaded by an external magnetic flux Φ_x and also connected to a gate voltage source V_g . We model the coplanar waveguide resonator as a series of LC circuits characterized by the capacitance and inductance per unit of length $c\Delta x$ and $l\Delta x$, respectively.

state

$$\rho_1^m(0) = |g\rangle\langle g| \bigotimes_{m=1}^M |0_m\rangle\langle 0_m|, \quad (19)$$

$$\rho_n^1(0) = \bigotimes_{n=1}^N |g_n\rangle\langle g_n| \otimes |0\rangle\langle 0|. \quad (20)$$

And let them evolve until t_f , and compute the fidelity \mathcal{F} at that time. For the GHZ cat state, we obtain that the fidelities for $M = 1$ and $M = 2$ is equal to $\mathcal{F} = \{0.998, 0.996\}$. Due to the constraints imposed by the size of the Hilbert space, we cannot explore the system, including more field modes. For the qubit-based GHZ state, we obtain that the fidelities are given by $\mathcal{F} = \{0.999, 0.998\}$ for $N = \{2, 4\}$, respectively. Since the coherence times are longer than the generation time, we do not observe an appreciable change in the optimal fidelity. We have performed our numerical simulation considering the same physical parameters as Fig. 1. For the decay rates we have chosen $\kappa/2\pi = 1$ MHz [77] for the field modes, and $\gamma/2\pi = 1/T_1$, with $T_1 = 40 \mu\text{s}$ and $\gamma_\phi/2\pi = 1/T_2$ with $T_2 = 40 \mu\text{s}$ [96] for the two-level system, respectively.

V. PHYSICAL IMPLEMENTATION

This section is devoted to the proposal of an experimental implementation based on cQED [96]. We will focus on the implementation of the Hamiltonian \mathcal{H}_n^m in Eq. (1). We depict the circuit implementation in Fig. 6(a) consisting into a

coplanar waveguide resonator (CPWR) [56] of length L and impedance $Z_0 = \sqrt{l/c}$ interrupted by M Josephson junctions of capacitance C_J and Josephson energy E_J that are uniformly distributed [97] along the CPWR. Furthermore, at the position $x = L$, we couple a flux-qubit [50–52] to the CPWR through the embedded junction. The flux-qubit consists of a superconducting loop with two Josephson junctions. We characterize the state of all the circuit constituents in terms of the flux $\psi(x, t) = \int_{-\infty}^t dt' V(x, t')$, with $V(x, t')$ as the voltage of the respective system component with respect to the surrounding ground plane. The circuit Lagrangian is given by

$$\mathcal{L} = \sum_{n=1}^N \mathcal{L}_{JJ}^{(n)} + \sum_{m=1}^{M+1} \mathcal{L}_{T1}^{(m)}, \quad (21)$$

where $\mathcal{L}_{JJ}^{(i)}$ is the Lagrangian of the flux-qubit coupled to a gate voltage defined as

$$\begin{aligned} \mathcal{L}_{JJ}^{(i)} = & \sum_{l=1}^3 \left[\frac{C_{J_l}^{(n)}}{2} (\dot{\phi}_l^{(n)})^2 + E_{J_l}^{(n)} \cos \left(\frac{\phi_l^{(n)}}{\varphi_0} \right) \right] \\ & + \frac{C_g^{(n)} (\phi_1^{(n)} - V_g^{(n)})^2}{2}, \end{aligned} \quad (22)$$

and $\mathcal{L}_{T1}^{(m)}$ is the Lagrangian describing CPWR

$$\mathcal{L}_{T1}^{(m)} = \sum_{j=0}^r \frac{c(\Delta x)}{2} (\dot{\psi}_j^{(m)})^2 - \sum_{k=0}^{r-1} \frac{(\psi_j^{(m)} - \psi_{r+1}^{(m)})^2}{2l(\Delta x)}. \quad (23)$$

Here $\psi_j^{(m)}$ and $\phi_l^{(m)}$ correspond to the flux variables describing the CPWR and the flux-qubit, respectively. We start our analysis by considering the qubit Lagrangian \mathcal{L}_Q . We can reduce the number of degree of freedom imposing the fluxoid quantization rule $\sum_l \varphi_l = 2n\pi + 2\pi f_x^m$ on the loop, where $\varphi_l = \phi_l/\varphi_0$ is the superconducting phase along the l th function with $\varphi_0 = \Phi_0/2\pi$ is the magnetic quantum flux, and $f_x^m = \Phi_x^m/\varphi_0$ is the frustration parameter. In this derivation, we assume that $E_{J_1}^{(m)} = E_{J_2}^{(m)} = E_J$, $E_{J_3}^{(m)} = \gamma E_J$, and $C_g = \epsilon C_J$. Moreover, we notice that $\phi_3^{(n)} \equiv \delta\psi$ corresponds to the flux on the CPWR at the position where the embedded junction is placed. After performing the fluxoid quantization rule, $\mathcal{L}_{JJ}^{(i)}$ turns into

$$\begin{aligned} \mathcal{L}_{JJ}^{(n)} = & \frac{C_J^{(n)} (2 + \gamma) (\dot{\phi}_1^{(n)})^2}{2} + (1 + \gamma) \frac{C_J^{(n)} (\delta\dot{\psi})^2}{2} \\ & - C_J^{(n)} \dot{\phi}_1^{(n)} \delta\dot{\psi} - \epsilon C_J^{(n)} \dot{\phi}_1^{(n)} V_g^{(n)} \\ & + E_J^{(n)} \left[\cos \left(\frac{\phi_1^{(n)}}{\varphi_0} \right) + \cos \left(\frac{\phi_1^{(n)} + \psi}{\varphi_0} - f_x^{(n)} \right) \right] \\ & + \gamma E_J^{(n)} \cos \left(\frac{\delta\psi}{\varphi_0} \right). \end{aligned} \quad (24)$$

From this expression, we can divide the Lagrangian into three main contributions

$$\mathcal{L}_{JJ}^{(n)} = \mathcal{L}_{\text{flux}}^{(n)} + \mathcal{L}_{\text{int}}^{(n)} + \mathcal{L}_{\text{emb}}^{(n)}, \quad (25)$$

each of them defined as follows

$$\mathcal{L}_{\text{flux}}^{(n)} = \frac{C_J^{(n)}(2 + \gamma)(\dot{\phi}_1^{(n)})^2}{2} - \delta C_J^{(n)} \dot{\phi}_1^{(n)} V_g^{(n)} \quad (26)$$

$$+ E_J^{(n)} \left[\cos\left(\frac{\phi_1^{(n)}}{\varphi_0}\right) + \cos\left(\frac{\phi_1^{(n)}}{\varphi_0} - f_x^{(n)}\right) \right],$$

$$\mathcal{L}_{\text{int}}^{(n)} = -C_J^{(n)} \dot{\phi}_1^{(n)} (\dot{\psi})$$

$$+ E_J^{(n)} \cos\left(\frac{\phi_1^{(n)}}{\varphi_0} - f_x^{(n)}\right) \frac{\delta\psi}{\varphi_0}, \quad (27)$$

$$\mathcal{L}_{\text{emb}}^{(m)} = (1 + \gamma) \frac{C_J^{(n)}(\dot{\delta\psi})^2}{2} + \gamma E_J^{(n)} \cos\left(\frac{\delta\psi}{\varphi_0}\right). \quad (28)$$

Lagrangian in Eq. (26) corresponds to the flux qubit Lagrangian, Eq. (27) is the capacitive and galvanic interaction between the embedded Josephson junction on the CPWR with the flux qubit, respectively. Finally, Lagrangian Eq. (28) is the embedded Josephson junction Lagrangian. Notice that in this derivation, we have assumed that $\delta\psi/\varphi_0 \ll 1$ is well localized, allowing us to expand the cosine up to second order. This limit is also known as the linearized regime of the Josephson junctions [97].

We proceed to calculate the Hamiltonian of the flux-qubit Lagrangian obtaining

$$\mathcal{H}_{\text{flux}}^{(n)} = \frac{(q^{(n)} - q_g^{(n)})^2}{2C_\Sigma^{(n)}} \quad (29)$$

$$- E_J^{(n)} \left[\cos\left(\frac{\phi^{(n)}}{\varphi_0}\right) + a \cos\left(\frac{\phi^{(n)}}{\varphi_0} - f_x^{(n)}\right) \right],$$

where $q^{(n)}$ is the canonical momenta of $\phi_1^{(n)}$, also $C_\Sigma = C_J^{(n)}(2 + \gamma)$ is the effective capacitance. Finally, $q_g^{(n)} = \delta C_J^{(n)} V_g^{(n)}$ is the gate charge of the flux qubit. The quantization is done by promoting quantum operators satisfying commutation relations $[\hat{N}, \exp(\pm i\hat{\theta})] = \exp(\pm i\theta)$ [98]. In such a case, we have $\hat{N}^{(n)} = -q^{(n)}/2e$, where $2e$ is the charge of a Cooper-pair, and $\hat{\theta}^{(n)} = \phi^{(n)}/\varphi_0$. On this basis, the quantum Hamiltonian reads

$$\hat{\mathcal{H}}_{\text{flux}}^{(n)} = 4E_C^{(n)}(\hat{N}^{(n)} - n_g^{(n)})^2 \quad (30)$$

$$- E_J^{(n)} [\cos(\hat{\theta}^{(n)}) - a \cos(\hat{\theta}^{(n)} - f_x^{(n)})],$$

where $E_C^{(n)} = e^2/2C_\Sigma^{(n)}$ is the charge energy, and $n_g^{(n)} = q_g^{(n)}/2e$ is the dimensionless charge gate. Thus, the circuit Hamiltonian takes the following short form

$$\hat{\mathcal{H}}_{\text{flux}}^{(n)} = 4E_C^{(n)}(\hat{N}^{(n)} - n_g^{(n)})^2$$

$$- E_J^{(n)}(f_x^{(n)}) \cos\left(\hat{\theta}^{(n)} - \frac{f_x^{(n)}}{2}\right), \quad (31)$$

where $E_J^{(n)}(f_x^{(n)}) = E_J^{(n)} \cos(f_x^{(n)}/2)$ is the tunable Josephson energy. We may extend the same analysis to the Lagrangian $\mathcal{L}_{\text{int}}^{(n)}$ noticing that in the usual working regime of the

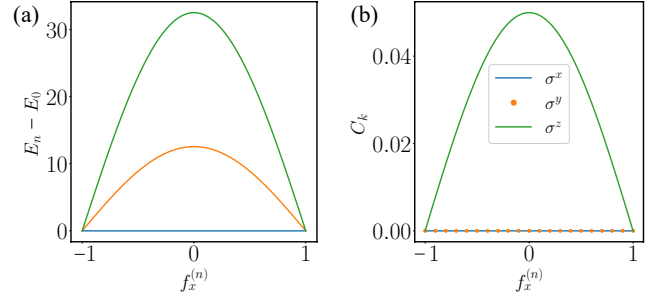


FIG. 7. Projection of the cosine operator in the Pauli matrix basis $\alpha_k = \text{Tr}[\sigma^k \cos(\hat{\theta}_J)]$ for the coupling operator as a function of the frustration parameter $f_x^{(n)}$. We have performed the simulation choosing the parameters $E_J/\hbar = 2\pi \times 20$ GHz, $E_C = E_J/67$, $E_\Sigma/\hbar = 2\pi \times 30$ GHz $\equiv 1.5 E_J$.

flux-qubit the capacitive interaction is smaller than the galvanic interaction [79]. In such a case, the interacting Hamiltonian is given by

$$\hat{\mathcal{H}}_{\text{int}}^{(n)} = -E_J^{(n)} \cos(\hat{\theta}^{(n)} - f_x^{(n)}) \frac{\psi_M^{(m)}}{\varphi_0}. \quad (32)$$

Now we proceed to calculate the Hamiltonian in Eq. (31) and Eq. (32) in the two-level approximation. For doing so, we consider only two charge states $N = \{0, 1\}$. In such basis we may write $\hat{\mathcal{H}}_{\text{flux}}^{(n)}$ as

$$\hat{\mathcal{H}}_{\text{flux}}^{(n)} = 4E_C^{(n)}(1 - 2n_g^{(n)})|e^{(n)}\rangle\langle e^{(n)}|$$

$$- E_J^{(n)}(f_x^{(n)}) \cos\left(\hat{\theta}^{(n)} - \frac{f_x^{(n)}}{2}\right). \quad (33)$$

Notice that by considering $n_g^{(n)} = 0.5$, we can see that the charge energy term vanishes and, more important both, the free term and the interaction term of the Hamiltonian have the same structure meaning that both terms will be identical in any basis. Fig. 7 shows the low-lying energy spectrum of the Hamiltonian $\hat{\mathcal{H}}_{\text{flux}}^{(n)}$ and the projection $C_k = \text{Tr}[\sigma^k \cos(\hat{\theta}^{(n)} - f_x^{(n)})]$ of the cosine operator on the Pauli matrices basis, as we can see the only non-zero projection corresponds to the operator σ .

We now derive the Hamiltonian of the coplanar waveguide resonator (CPWR) with the embedded Josephson junction described by the Lagrangian

$$\mathcal{L}_{\text{TI}}^{(m)} + \mathcal{L}_{\text{emb}}^{(m)} =$$

$$\sum_{j=0}^r \frac{c(\Delta x)}{2} (\dot{\psi}_j^{(m)})^2 - \sum_{j=0}^{r-1} \frac{(\psi_j^{(m)} - \psi_{j+1}^{(m)})^2}{2l(\Delta x)}.$$

$$+ (1 + \gamma) \frac{C_J^{(n)}(\dot{\delta\psi})^2}{2} + \gamma E_J^{(n)} \cos\left(\frac{\delta\psi}{\varphi_0}\right). \quad (34)$$

A good strategy to find the Hamiltonian of the CPWR is to add and subtract an harmonic term $\pm(\psi_M^{(m)})^2/2L_J^{(m)}$, where

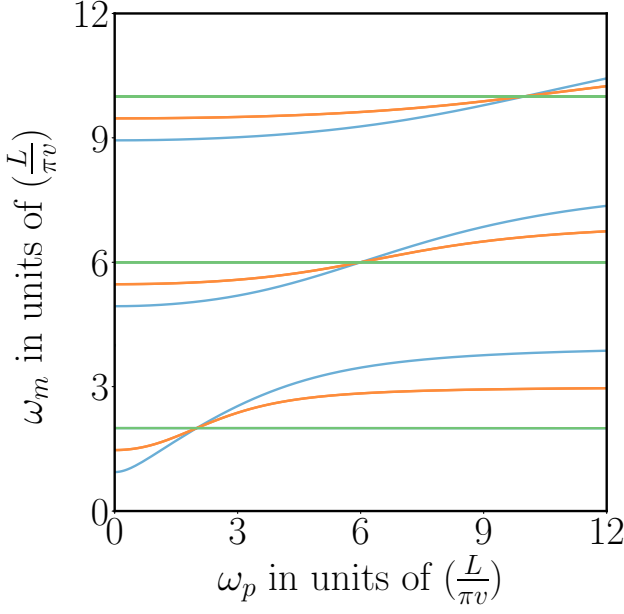


FIG. 8. Energy spectrum of the coplanar waveguide resonator with three Josephson junction embedded on it as a function of the plasma frequency ω_p . The system parameter are $v = 0.98 \times 10^8$ m/s, $Z_0 = 50\Omega$, $C_J = 1$ pF and $L = 0.28$ mm. For a specific value of plasma frequency, the eigenmode of the CPWR becomes degenerate.

$L_J^{(m)} = \varphi_0^2 / E_J^{(m)}$ is the Josephson inductance. Thus, we can divide the embedded junction Lagrangian into its harmonic and anharmonic parts. Notice that this procedure is the same as expanding the cosine term up to the lowest contribution (the linearized regime) [99]. We proceed by computing the Euler-Lagrange equation for the CPWR for both edges ($x = 0$ and $x = L$) and, in the bulk, obtaining the following equations

$$(c\Delta x)\ddot{\psi}_0^{(1)} = \frac{-1}{l(\Delta x)}(\psi_0^{(1)} - \psi_1^{(m)})|_{x=0}, \quad (35)$$

$$(c\Delta x)\ddot{\psi}_m^{(M+1)} = \frac{1}{l(\Delta x)}(\psi_{m-1}^{(M+1)} - \psi_m^{(M+1)})|_{x=L}, \quad (36)$$

$$(c\Delta x)\ddot{\psi}_q^{(m)} = \frac{1}{l(\Delta x)}(2\psi_q^{(m)} - \psi_{q+1}^{(m)} - \psi_{q-1}^{(m)}). \quad (37)$$

Another equation of motion appears when we calculate the Euler-Lagrange equation at the position where the embedded junction is placed.

$$c(\Delta x)\ddot{\psi}_m^{(m)} + (a + \gamma)(\ddot{\psi}_n^{(m)} - \ddot{\psi}_0^{(m+1)}) = \frac{-1}{l(\Delta x)}(\psi_{m-1}^{(m)} - \psi_m^{(m)}) - \frac{1}{L_J^{(m)}}(\psi_m^{(m)} - \psi_0^{(m+1)}). \quad (38)$$

To solve the set of equations, we take the continuum limit ($\Delta x \rightarrow 0$), and the flux $\psi \rightarrow \psi(x, t)$ turns into a smooth function of the position and time. Under such limit, we obtain

the following eigenvalue problem [99]:

$$\partial_t^2 \psi(x, t) = v^2 \partial_x^2 \psi(x, t), \quad (39a)$$

$$\frac{1}{l} \partial_x \psi(x, t)|_{x=0} = 0, \quad (39b)$$

$$\frac{1}{l} \partial_x \psi(x, t)|_{x=L} = 0, \quad (39c)$$

$$-\partial_x \psi(x = jb, t) = l(1 + \gamma)C_J^{(i)} \delta \ddot{\psi} - \frac{\delta \psi}{L_J^{(i)}}, \quad (39d)$$

where $v = 1/\sqrt{lc}$ is the wave velocity. $x = jb$ with $b = L/(N + 1)$ as the position of each Josephson junction and the spacing between them, respectively. Moreover, $\delta \psi^{(i)} = \psi_n^{(i)} - \psi_0^{(i+1)}$ is flux approaching the junction from the left $\psi_n^{(i)}$ and from the right $\psi_0^{(i+1)}$. With all the above expressions, we found the transcendental equation for the CPWR frequencies, given by

$$-\partial_x \psi(x = jb, t) = \frac{l}{L_J^{(i)}} \left(1 - \frac{(1 + \gamma)\omega_r^2}{\omega_p^2} \right) \delta \psi, \quad (40)$$

where $\omega_p = 1/\sqrt{C_J^{(m)} L_J^{(m)}}$ is the plasma frequency of the m th Josephson junction. We obtain the quantum Hamiltonian assuming a normal mode expansion of the form $\psi(x, t) = \sum_r g_r(t) f_r(x)$ and $f_r(x) = A_r(x) + B_r(x)$ that leads to the following Hamiltonian

$$H_{\text{CPWR}} = \sum_m \frac{\pi_m^2}{2\eta_m} + \frac{\eta_m \omega_m^2 g_m^2}{2} + H_{\text{nonlin}}. \quad (41)$$

Here $\pi_r = \eta_r \dot{g}_r$ is the canonical conjugate momenta of g_r , $\eta_r = \int_0^L (c f_r^2 dx + \sum_{i=1}^{N+1} (1 + \gamma) C_J^{(i)} [\delta f_r]^2)$ is the effective mass of the r -th eigenmode and ω_m is the frequency associated with the m -th eigenmode that is solution of the transcendental equation in Eq. (39d) which corresponds to

$$\frac{\cos\left(\frac{\omega_m b}{v}\right) - \cos\left(\frac{n\pi}{N+1}\right)}{\sin\left(\frac{\omega_m b}{v}\right)} = \frac{1}{2C_J Z_0} \frac{\omega_m}{(\omega_p^2 - (1 + \gamma)\omega_m^2)}. \quad (42)$$

In Fig. 8 we plot the solution of Eq. (42) as a function of the plasma frequency for a CPWR containing two Josephson junctions. From the solution, we observe that many degenerate manifolds exist on the CPWR as embedded Josephson junctions. Thus, for having a set of M modes with the same frequency, we require M embedded junctions. The Hamiltonian in Eq. (41) is quantized by promoting the following quantum operators defined as $a_r = \sqrt{\eta_r \omega_r / 2} (g_r + i\pi_r / \eta_r \omega_r)$ for each eigenmode of the manifold, arriving the following Hamiltonian

$$H_{\text{CPWR}} = \sum_m \hbar \omega_m a_m^\dagger a_m + H_{\text{nonlin}}, \quad (43)$$

which allows us to write the Hamiltonian of the system as follows

$$\mathcal{H} = \sum_{m=1}^M \hbar \omega_m a_m^\dagger a_m + \sum_{n=1}^N \frac{\hbar \Omega}{2} \sigma_n^z + \sum_{n,m} g_n^m \sigma_n^z (a_m^\dagger + a_m),$$

with the coupling strength being $g_n^m = E_J^{(m)}(f_x^{(m)})\sqrt{\frac{2}{N+1}}\sin(\frac{\pi j}{N+1})\lambda(\omega_m)$ and $\lambda(\omega_m)$ depending on the circuital parameters [99]. Notice that by rotating the system on the y axis, we obtain the Hamiltonian in Eq. (6). Thus, a quantum platform to generate multipartite entangled states relies on a coplanar waveguide resonator coupled to several flux-qubit with embedded junctions to have degenerate manifold field mode frequencies.

VI. CONCLUSION

In this article, we have proposed the reverse-engineering method to design a longitudinal interaction to generate multipartite entangled states in photonic and qubit-based systems. Such approach suggests a modulation that satisfies the desired criteria under suitable conditions. In our case, we constrain the modulation to achieve a fixed cavity displacement to generate photonic multi-partite entangled states. In contrast, we impose the vanishing of some unwanted interaction to implement a Sørensen-Mølmer quantum gate to generate multi-partite qubit states, respectively. As a result, we obtain a fast generation time (less than tens of nanoseconds) with the current state-of-the-art superconducting quantum circuits architecture. Notably, the gating time does not scale with the number of either field modes or qubits, allowing us to generate entangled quantum states containing many parties. Since

the generation time is shorter than the coherence time of the subsystem, the unavoidable effect of the environment does not induce a significantly detrimental impact on the final fidelity generation. The renewed attention to the protocols provided by STA in the context of cQED may pave the way to accelerate and improve several quantum tasks by engineering the adequate pulses sequences and modulation that are fundamentally constrained in the quantum platform.

ACKNOWLEDGMENTS

This work was financially supported by NSFC (12075145), STCSM (Grant No. 2019SHZDZX01-ZX04), EU FET Open Grant EPIQUS (Grant No. 899368), the Basque Government through Grant No. IT1470-22, the project grant PID2021-126273NB-I00 funded by MCIN/AEI/10.13039/501100011033 and by “ERDF A way of making Europe” and “ERDF Invest in your Future”, and QUANTEK project (Grant No. KK-2021/00070). F. A. C. L. thanks to the German Ministry for Education and Research, under QSolid, Grant no. 13N16149. J.C. acknowledges to Financiamiento Basal para Centros Científicos y Tecnológicos de Excelencia (Grant No. AFB180001). X.C. acknowledges ayudas para contratos Ramón y Cajal–2015–2020 (RYC-2017-22482).

-
- [1] R. Horodecki, P. Horodecki, M. Horodecki, and K. Horodecki, Quantum entanglement, *Rev. Mod. Phys.* **81**, 865 (2009).
 - [2] G. Adesso, T. R. Bromley, and M. Cianciaruso, Measures and applications of quantum correlations, *J. Phys. A: Math. Theor.* **49** 473001 (2016).
 - [3] S.-B. Zheng, and G.-C. Guo, Efficient Scheme for Two-Atom Entanglement and Quantum Information Processing in Cavity QED, *Phys. Rev. Lett.* **85**, 2392 (2000).
 - [4] C. Monroe, Quantum information processing with atoms and photons, *Nature* **416**, 238 (2002).
 - [5] C. H. Bennett, and D. P. DiVincenzo, Quantum information and computation, *Nature* **404**, 247 (2000).
 - [6] R. Feynman, Simulating physics with computers, *Int. J. Theor. Phys.* **21**, 467 (1982).
 - [7] A. Ekert, R. Jozsa, Quantum algorithms: entanglement enhanced information processing, *Philos. Trans. Royal Soc. A* **356**, 1769 (1998).
 - [8] D. Deutsch, and R. Jozsa, Rapid solutions of problems by quantum computation, *Proceedings of the Royal Society of London A* **439**: 553 (1992).
 - [9] S. Beauregard, Circuit for Shor’s algorithm using $2n+3$ qubits, *arXiv:quant-ph/0205095*.
 - [10] L. K. Grover, A fast quantum mechanical algorithm for database search, *Proceedings of the 28th Annual ACM Symposium on the Theory of Computing (STOC 1996)*.
 - [11] R. Cleve, A. Ekert, C. Macchiavello, M. Mosca, Quantum algorithms revisited, *Proceedings of the Royal Society of London A* **454**: 339 (1998).
 - [12] U. Schollwöck, The density-matrix renormalization group, *Rev. Mod. Phys.* **77**, 259 (2005).
 - [13] S. R. White, Density-matrix algorithms for quantum renormalization groups, *Phys. Rev. B* **48**, 10345 (1993).
 - [14] T. J. Osborne and M. A. Nielsen, Entanglement in a simple quantum phase transition, *Phys. Rev. A* **66**, 032110 (2002).
 - [15] A. Osterloh, L. Amico, G. Falci, and R. Fazio, Scaling of entanglement close to a quantum phase transition, *Nature* **416**, 608 (2002).
 - [16] S.-J. Gu, S.-S. Deng, Y.-Q. Li, and H.-Q. Lin, Entanglement and Quantum Phase Transition in the Extended Hubbard Model, *Phys. Rev. Lett.* **93**, 086402 (2004).
 - [17] T. Werlang, C. Trippe, G. A. P. Ribeiro, and G. Rigolin, Quantum Correlations in Spin Chains at Finite Temperatures and Quantum Phase Transitions, *Phys. Rev. Lett.* **105**, 095702 (2010).
 - [18] V. Giovannetti, S. Lloyd, and L. Maccone, Quantum Metrology, *Phys. Rev. Lett.* **96**, 010401 (2006).
 - [19] S. Boixo, A. Datta, M. J. Davis, S. T. Flammia, A. Shaji, and C. M. Caves, Quantum Metrology: Dynamics versus Entanglement, *Phys. Rev. Lett.* **101**, 040403 (2008).
 - [20] M. F. Riedel, P. Böhi, Y. Li, T. W. Hänsch, A. Sinatra, and P. Treutlein, Atom-chip-based generation of entanglement for quantum metrology, *Nature* **464**, 1170 (2010).
 - [21] C. D. Bruzewicz, J. Chiaverini, R. McConnell, J. M. Sage, Trapped-Ion Quantum Computing: Progress and Challenges, *Appl. Phys. Rev.* **6**, 021314 (2019).
 - [22] K. Mølmer and A. Sørensen, Quantum Computation with Ions in Thermal Motion, *Phys. Rev. Lett.* **82**, (1971).

- [23] K. Mølmer and A. Sørensen, Multiparticle Entanglement of Hot Trapped Ions, *Phys. Rev. Lett.* **82**, (1971).
- [24] X. Wang, A. Sørensen, and K. Mølmer, Multibit Gates for Quantum Computing, *Phys. Rev. Lett.* **86**, 3907 (2001).
- [25] J. J. García-Ripoll, P. Zoller, and J. I. Cirac, Speed Optimized Two-Qubit Gates with Laser Coherent Control Techniques for Ion Trap Quantum Computing, *Phys. Rev. Lett.* **91**, 157901 (2003).
- [26] J. J. García-Ripoll, P. Zoller, and J. I. Cirac, Coherent control of trapped ions using off-resonant lasers, *Phys. Rev. A* **71**, 062309 (2005).
- [27] M. H. Devoret, J. M. Martinis, Implementing Qubits with Superconducting Integrated Circuits, *Experimental Aspects of Quantum Computing*, Springer, Boston, MA (2005).
- [28] J. Q. You, F. Nori, Superconducting Circuits and Quantum Information, *Phys. Today* **58**, 42 (2005).
- [29] J. Clarke and F. K. Wilhelm, Superconducting quantum bits, *Nature* **453**, 1031 (2008).
- [30] G. Wendin, and V.S. Shumeiko, Superconducting Quantum Circuits, Qubits and Computing, [arXiv:cond-mat/0508729](https://arxiv.org/abs/cond-mat/0508729) [**cond-mat.supr-con**] (2005).
- [31] M. H. Devoret, and R. J. Schoelkopf, Superconducting Circuits for Quantum Information: An Outlook, *Science*, **339**, 1169 (2013).
- [32] A. F. Kockum, and F. Nori, Quantum Bits with Josephson Junctions, *Fundamentals and Frontiers of the Josephson Effect*, Springer Series in Materials Science, Vol 286. Springer, Cham. (2019).
- [33] P. Krantz, M. Kjaergaard, F. Yan, T. P. Orlando, S. Gustavsson, W. D. Oliver, A Quantum Engineer's Guide to Superconducting Qubits, *Applied Physics Reviews* **6**, 021318 (2019).
- [34] M. Kjaergaard, M. E. Schwartz, J. Braumüller, P. Krantz, J. I. J. Wang, S. Gustavsson, and W. D. Oliver, Superconducting qubits: Current state of play, *Annual Review of Condensed Matter Physics*, **11**, 369 (2020).
- [35] J. M. Martinis, M. H. Devoret, and J. Clarke, Quantum Josephson junction circuits and the dawn of artificial atoms, *Nature Physics* **16**, 234 (2020).
- [36] A. Blais, R.-S. Huang, A. Wallraff, S. M. Girvin, and R. J. Schoelkopf, Cavity quantum electrodynamics for superconducting electrical circuits: An architecture for quantum computation, *Phys. Rev. A* **69**, 062320 (2004).
- [37] A. Wallraff, D. I. Schuster, A. Blais, L. Frunzio, R.-S. Huang, J. Majer, S. Kumar, S. M. Girvin, and R. J. Schoelkopf, Strong coupling of a single photon to a superconducting qubit using circuit quantum electrodynamics, *Nature* **431**, 162 (2004).
- [38] I. Chiorescu, P. Bertet, K. Semba, Y. Nakamura, C. J. P. M. Harmans, and J. E. Mooij, Coherent dynamics of a flux qubit coupled to a harmonic oscillator, *Nature* **431**, 159 (2004).
- [39] R. J. Schoelkopf and S. M. Girvin, Wiring up quantum systems, *Nature* **451**, 664 (2008).
- [40] A. Blais, A. L. Grimsmo, S. M. Girvin, and, A. Wallraff, Circuit quantum electrodynamics, *Rev. Mod. Phys.* **93**, 025005 (2021).
- [41] A. Blais, S. M. Girvin, and W. D. Oliver, Quantum information processing and quantum optics with circuit quantum electrodynamics, *Nature Physics* **16**, 247 (2020).
- [42] V. Bouchiat, D. Vion, P. Joyez, D. Esteve, and M. H. Devoret, *Phys. Scr.* **1998**, 165 (1998).
- [43] Y. Nakamura, Yu. Pashkin and J. S. Tsai, *Nature* **398**, 786 (1999).
- [44] J. Koch, T. M. Yu, J. Gambetta, A. A. Houck, D. I. Schuster, J. Majer, A. Blais, M. H. Devoret, S. M. Girvin, and R. J. Schoelkopf, *Phys. Rev. A* **76**, 042319 (2007).
- [45] J. A. Schreier, A. A. Houck, J. Koch, D. I. Schuster, B. R. Johnson, J. M. Chow, J. M. Gambetta, J. Majer, L. Frunzio, M. H. Devoret, S. M. Girvin, and R. J. Schoelkopf, *Phys. Rev. B* **77**, 180502(R) (2008).
- [46] R. Barends, J. Kelly, A. Megrant, D. Sank, E. Jeffrey, Y. Chen, Y. Yin, B. Chiaro, J. Mutus, C. Neill, P. O'Malley, P. Roushan, J. Wenner, T. C. White, A. N. Cleland, and J. M. Martinis, *Phys. Rev. Lett.* **111**, 080502 (2013).
- [47] J. M. Martinis, S. Nam, J. Aumentado, and C. Urbina, *Phys. Rev. Lett.* **89**, 117901 (2002).
- [48] M. Steffen, M. Ansmann, R. McDermott, N. Katz, R. C. Bialczak, E. Lucero, M. Neeley, E. M. Weig, A. N. Cleland, and J. M. Martinis, *Phys. Rev. Lett.* **97**, 050502 (2006).
- [49] M. Ansmann, H. Wang, R. C. Bialczak, M. Hofheinz, E. Lucero, M. Neeley, A. D. O'Connell, D. Sank, M. Weides, J. Wenner, A. N. Cleland, and J. M. Martinis, *Nature* **461**, 504 (2009).
- [50] T. P. Orlando, J. E. Mooij, L. Tian, C. H. van der Wal, L. S. Levitov, S. Lloyd, and J. J. Mazo, *Phys. Rev. B* **60**, 15398 (1999).
- [51] J. E. Mooij, T. P. Orlando, L. Levitov, L. Tian, C. H. van der Wal, and S. Lloyd, *Science* **285**, 1036 (1999).
- [52] A. V. Shcherbakova, K. G. Fedorov, K. V. Shulga, V. V. Ryazanov, V. V. Bolginov, V. A. Oboznov, S. V. Egorov, V. O. Shkolnikov, and M. J. Wolf, D. Beckmann, *Supercond. Sci. Technol.* **28**, 025009 (2015).
- [53] S. M. Girvin, *Circuit QED: superconducting qubits coupled to microwave photons* (Vol. 96) (M. Devoret, B. Huard, R. Schoelkopf, L. F. Cugliandolo, Oxford, 2014).
- [54] A.F. Kockum, F. Nori, *Springer Series in Materials Science* **286**, Chapter 17, pp. 703-741 (2019).
- [55] T. Itoh, *IEEE Trans. Microwave Theory Tech.* **22**, 946 (1974).
- [56] M. Göppl, A. Fragner, M. Baur, R. Bianchetti, S. Filipp, J. M. Fink, P. J. Leek, G. Puebla, L. Steffen, and A. Wallraff, *J. Appl. Phys.* **104**, 113904 (2008).
- [57] M. F. Gely, A. Parra-Rodriguez, D. Bothner, Y. M. Blanter, S. J. Bosman, E. Solano, and G. A. Steele, *Phys. Rev. B* **95**, 245115 (2017).
- [58] R. Migliore, K. Yuasa, H. Nakazato, and A. Messina, Generation of multipartite entangled states in Josephson architectures, *Phys. Rev. B* **74**, 104503 (2006).
- [59] Y. -D. Wang, S. Chesi, D. Loss, and C. Bruder, One-step multi-qubit Greenberger-Horne-Zeilinger state generation in a circuit QED system, *Phys. Rev. B* **81**, 10452 (2010).
- [60] C. Wu, C. Guo, Y. Wang, G. Wang, X.-L. Feng, and J.-L. Chen, Generation of Dicke states in the ultrastrong-coupling regime of circuit QED systems, *Phys. Rev. A* **95**, 013845 (2017).
- [61] J. Li, G. Wang, R. Xiao, C. Sun, C. Wu, and K. Xue, Multi-qubit Quantum Rabi Model and Multi-partite Entangled States in a Circuit QED System, *Scientific Reports* **9**, 1380 (2019).
- [62] C. Simon and J. Kempe, Robustness of multiparty entanglement, *Phys. Rev. A* **65**, 052327 (2002).
- [63] T. Yu and J. H. Eberly, Phonon decoherence of quantum entanglement: Robust and fragile states, *Phys. Rev. B* **66**, 193306 (2002).
- [64] A. R. R. Carvalho, F. Mintert, and A. Buchleitner, Decoherence and Multipartite Entanglement, *Phys. Rev. Lett.* **93**, 230501 (2004).
- [65] J. Novotný, Gernot Alber, and I. Jex, Entanglement and Decoherence: Fragile and Robust Entanglement, *Phys. Rev. Lett.* **107**, 090501 (2011).
- [66] A.F. Kockum, A. Miranowicz, S. De Liberato, S. Savasta, F. Nori, *Nat. Rev. Phys.* **1**, 19 (2019).
- [67] P. Forn-Díaz, L. Lamata, E. Rico, J. Kono, and E. Solano, *Rev. Mod. Phys.* **91**, 025005 (2019).

- [68] J. Casanova, G. Romero, I. Lizuain, J. J. García-Ripoll, and E. Solano, *Phys. Rev. Lett.* **105**, 263603 (2010).
- [69] F. Yoshihara, T. Fuse, S. Ashhab, K. Kakuyanagi, S. Saito, and K. Semba, *Nat. Phys.* **12**, 44 (2017).
- [70] Xi. Chen, A. Ruschhaupt, S. Schmidt, A. del Campo, D. Guéry-Odelin, and J. G. Muga, Fast Optimal Frictionless Atom Cooling in Harmonic Traps: Shortcut to Adiabaticity, *Phys. Rev. Lett.* **104**, 063002 (2010).
- [71] D. Guéry-Odelin, A. Ruschhaupt, A. Kiely, E. Torrontegui, Shortcuts to adiabaticity: Concepts, methods, and applications, *Rev. Mod. Phys.* **91**, 045001 (2019).
- [72] R. Dann, A. Tobalina, and R. Kosloff, Shortcut to Equilibration of an Open Quantum System, *Phys. Rev. Lett.* **122**, 250402 (2019).
- [73] S. Alipour, A. Chenu, A. T. Rezakhani⁴, and A. del Campo, Shortcuts to Adiabaticity in Driven Open Quantum Systems: Balanced Gain and Loss and Non-Markovian Evolution, *Quantum* **4**, 336 (2020).
- [74] Zelong Yin, Chunzhen Li, Jonathan Allcock, Yicong Zheng, Xiu Gu, Maochun Dai, Shengyu Zhang, Shuoming An, Shortcuts to Adiabaticity for Open Systems in Circuit Quantum Electrodynamics, *Nat. Commun* **13**, 188 (2022).
- [75] F. A. Cárdenas-López and Xi Chen, Shortcuts to adiabaticity for fast qubit readout in circuit quantum electrodynamics, *Phys. Rev. Appl.* **accepted**, (2022).
- [76] Jia-Xin Li, F. A. Cárdenas-López and Xi Chen, to be published.
- [77] N. Didier, J. Bourassa, and A. Blais, Fast Quantum Nondemolition Readout by Parametric Modulation of Longitudinal Qubit-Oscillator Interaction, *Phys. Rev. Lett.* **115**, 203601 (2015).
- [78] D. Kafri, C. Quintana, Y. Chen, A. Shabani, J. M. Martinis, and H. Neven, Tunable inductive coupling of superconducting qubits in the strongly nonlinear regime, *Phys. Rev. A* **95**, 052333 (2017).
- [79] J. Bourassa, J. M. Gambetta, A. A. Abdumalikov, Jr., O. Astafiev, Y. Nakamura, and A. Blais, Ultrastrong coupling regime of cavity QED with phase-biased flux qubits, *Phys. Rev. A* **80**, 032109 (2009).
- [80] P.-M. Billangeon, J. S. Tsai, and Y. Nakamura, Circuit-QED-based scalable architectures for quantum information processing with superconducting qubits, *Phys. Rev. B* **91**, 094517 (2015).
- [81] B. Wang, L.-M. Duan, Engineering superpositions of coherent states in coherent optical pulses through cavity-assisted interaction. *Phys. Rev. A* **72**, 022320 (2005).
- [82] M. Brune, E. Hagley, J. Dreyer, X. Maître, A. Maali, C. Wunderlich, J. M. Raimond, and S. Haroche, Observing the Progressive Decoherence of the “Meter” in a Quantum Measurement, *Phys. Rev. Lett.* **77**, 4887 (1996).
- [83] L. Sun, A. Petrenko, Z. Leghtas, B. Vlastakis, G. Kirchmair, K. M. Sliwa, A. Narla, M. Hatridge, S. Shankar, J. Blumoff, L. Frunzio, M. Mirrahimi, M. H. Devoret, and R. J. Schoelkopf, Tracking photon jumps with repeated quantum non-demolition parity measurements, *Nature* **511**, 444 (2014).
- [84] B. Vlastakis, G. Kirchmair, Z. Leghtas, S. E. Nigg, L. Frunzio, S. M. Girvin, M. Mirrahimi, M. H. Devoret, R. J. Schoelkopf, Deterministically Encoding Quantum Information Using 100-Photon Schrödinger Cat States, *Science* **342**, 607 (2013).
- [85] M. O. Scully, and M. S. Zubairy, Quantum Optics, *Cambridge University Press, Cambridge, England*, (1997).
- [86] M.A. Nielsen, and I. L. Chuang, *Quantum computation and quantum information* (Cambridge University Press, UK, 2000).
- [87] W. Rossmann, Lie Groups – An Introduction Through Linear Groups, Oxford Graduate Texts in Mathematics, Oxford Science Publications (2002).
- [88] R. Barends, L. Lamata, J. Kelly, L. García-Álvarez, A. G. Fowler, A. Megrant, E. Jeffrey, T. C. White, D. Sank, J. Y. Mutus, B. Campbell, Yu Chen, Z. Chen, B. Chiaro, A. Dunsworth, I.-C. Hoi, C. Neill, P. J. J. O’Malley, C. Quintana, P. Roushan, A. Vainsencher, J. Wenner, E. Solano, and J. M. Martinis, Digital quantum simulation of fermionic models with a superconducting circuit, *Nat. Comm.* **6**, 7654 (2015).
- [89] G. Zhu, Y. Subasi, J. D. Whitfield, and M. Hafezi, Hardware-efficient fermionic simulation with a cavity-QED system, *npj Quantum Information* **4**, 16 (2018).
- [90] W. Dür, G. Vidal, and J. I. Cirac, Three qubits can be entangled in two inequivalent ways, *Phys. Rev. A* **62**, 062314 (2000).
- [91] X. Chen, R.-L. Jiang, J. Li, Y. Ban, and E. Ya. Sherman, Inverse engineering for fast transport and spin control of spin-orbit-coupled Bose-Einstein condensates in moving harmonic traps, *Phys. Rev. A* **97**, 013631 (2018).
- [92] T. Čadež, J. H. Jefferson, and A. Ramšak, A non-adiabatically driven electron in a quantum wire with spin-orbit interaction, *New J. Phys.* **15**, 013029 (2013).
- [93] T. Čadež, J. H. Jefferson, and A. Ramšak, Exact Nonadiabatic Holonomic Transformations of Spin-Orbit Qubits, *Phys. Rev. Lett.* **112**, 150402 (2014).
- [94] Online documentation `scipy.optimize.minimize(method='CG')`
- [95] H. P. Breuer and F. Petruccione, *The Theory of Open Quantum Systems* (Oxford University Press, Oxford, 2002).
- [96] G. Wendin, Quantum information processing with superconducting circuits: a review, *Rep. Prog. Phys.* **80**, 106001 (2017).
- [97] M. Leib, and M. J. Hartmann, Synchronized Switching in a Josephson Junction Crystal, *Phys. Rev. Lett.* **112**, 223603 (2014).
- [98] A. Cottet, *Implementation of a quantum bit in a superconducting circuit*, Ph.D. Thesis (2002).
- [99] M. Leib and M. J. Hartmann, Synchronized Switching in a Josephson Junction Crystal, *Phys. Rev. Lett.* **112**, 223603 (2014).